Continuous cross-over from ferroelectric to relaxor state and piezoelectric properties of BaTiO3-BaZrO3-CaTiO3 single crystals

Feres Benabdallah, Philippe Veber, Mythili Prakasam, Oudomsack Viraphong, Kiyoshi Shimamura, Mario Maglione

Continuous cross-over from ferroelectric to relaxor state and piezoelectric properties of BaTiO3-BaZrO3-CaTiO3 single crystals

F. Benabdallah, P. Veber, M. Prakasam, O. Viraphong, K. Shimamura, and M. Maglione

Citation: Journal of Applied Physics **115**, 144102 (2014); doi: 10.1063/1.4870933
View online: http://dx.doi.org/10.1063/1.4870933
View Table of Contents: http://scitation.aip.org/content/aip/journal/jap/115/14?ver=pdfcov
Published by the AIP Publishing

JOURNAL OF APPLIED PHYSICS **115**, 144102 (2014)

Continuous cross-over from ferroelectric to relaxor state and piezoelectric properties of $BaTiO_3$-$BaZrO_3$-$CaTiO_3$ single crystals

F. Benabdallah,[1,2] P. Veber,[1,2,a)] M. Prakasam,[1,2] O. Viraphong,[1,2] K. Shimamura,[3] and M. Maglione[1,2]
[1]*CNRS, ICMCB, UPR 9048, F-33600 Pessac, France*
[2]*Université Bordeaux, ICMCB, UPR 9048, F-33600 Pessac, France*
[3]*National Institute for Materials Science (NIMS), 1-1 Namiki, Tsukuba, Ibaraki 305-0044, Japan*

(Received 14 February 2014; accepted 29 March 2014; published online 8 April 2014)

Optimal properties like piezoelectricity can be found in polarizable materials for which the structure changes sharply under small composition variations in the vicinity of their morphotropic phase boundary or the triple point in their isobaric temperature-composition phase diagram. In the latter, lead-free $(Ba_{0.850}Ca_{0.150})(Ti_{0.900}Zr_{0.100})O_3$ ceramics exhibit outstanding piezoelectric coefficients. For the first time, we report the growth of piezoelectric lead-free single crystals in the $BaTiO_3$-$BaZrO_3$-$CaTiO_3$ pseudo-ternary system. The stoichiometry control in the CaO-BaO-TiO_2-ZrO_2 solid solution led to single crystals with various compositions ranging from $(Ba_{0.857}Ca_{0.143})(Ti_{0.928}Zr_{0.072})O_3$ to $(Ba_{0.953}Ca_{0.047})(Ti_{0.427}Zr_{0.573})O_3$. We evidenced a continuous cross-over from a ferroelectric state at high titanium content to a relaxor one on increasing the zirconium content. Such a property tuning is rather seldom observed in lead-free ferroelectrics and confirms what was already reported for ceramics. Single crystal with $(Ba_{0.838}Ca_{0.162})(Ti_{0.854}Zr_{0.146})O_3$ composition, which has been grown and oriented along [001] crystallographic direction, displayed electromechanical coefficients d_{31} and k_{31} of 93 $pC.N^{-1}$ and 0.18, respectively, near the room temperature (T = 305 K). © *2014 AIP Publishing LLC*. [http://dx.doi.org/10.1063/1.4870933]

I. INTRODUCTION

Investigations of oxides and ionic materials, in particular, ABO_3 perovskites, are a rich source for the understanding of structural mechanisms. Beyond their fundamental interest, perovskites attract attention as functional oxides, often related to ferroelectric, piezoelectric, or multiferroic properties.[1,2] The ideal cubic (C) structure of ABO_3 perovskites is rather simple with corner-linked BO_6 octahedra and the A cations sitting in the space between the octahedra.[3] However, most perovskites present structural distortions away from this parent cubic structure, which can be driven by external stresses or chemical substitution. One of the major challenges in perovskite science is the identification of these usually subtle distortions and to correlate them to their physical properties. The prototype example of a complex perovskite with a great relevance to both fundamental and application-related issues is the industrial piezoelectric standard $PbZr_{1-x}Ti_xO_3$ (PZT).[1] Even though thoroughly studied since 1960s, it was only in 1998 that Noheda and co-workers provided through high resolution synchrotron powder diffraction, an understanding of the observed phase transitions and the underlying mechanism of the important piezoelectric response.[4,5] A step further was achieved soon after when larger piezoelectric coefficients were found at the intermediate stage between two polar states. This was again in lead-containing solid solutions, the archetype of which is $PbMg_{1/3}Nb_{2/3}O_3$-$PbTiO_3$ (PMN-PT), where the cross over from PMN relaxor to PT ferroelectric is the composition range of interest.[6–8]

An important amount of the current research in the field of piezoelectrics aims at the replacement of PZT and other lead-containing perovskites by equally good piezoelectrics, which contain no Pb, thus by more environmental-friendly materials. Unfortunately, lead-free alternatives to PZT are extremely rare and restricted to solid solutions derived from bismuth-based $(Na_{1/2}Bi_{1/2}TiO_3)$[9,10] and alkali-based ($KNbO_3$, $NaNbO_3$)[11–13] compounds. Considering all of them, the combination of two or three different crystal structures lead automatically to a flattening Gibbs free energy and gives rise consequently to a large piezoelectric response via polarization rotation or polarization extension mechanisms.[14]

In 2009, Liu *et al.*[15] reported a complex pseudo-binary system $(1-x)BaTi_{0.8}Zr_{0.2}O_3$-$xBa_{0.7}Ca_{0.3}TiO_3$ (BCTZ) in polycrystalline form with a surprisingly high piezoelectric coefficient $d_{33} = 620$ $pC.N^{-1}$, comparable to that of PZT at room temperature. Our own study of high-quality samples has recently confirmed these high values.[16] For a full understanding of the microscopic origins of these outstanding properties, such as local composition fluctuations, phase coexistence, or polarization flexibility, we undertook the growth of BCTZ single crystals focusing on compositions close to $(Ba_{0.850}Ca_{0.150})(Ti_{0.900}Zr_{0.100})O_3$ (x = 0.5) for which the largest piezoelectric coefficients have been reported. Within this context, we were inspired by many excellent contributions, which had provided unambiguous responses about crystallographic structure evolutions and domain configurations in both lead-containing and lead-free perovskite-structured single crystals such as PZT (with x = 0.325 and x = 0.460),[17,18] PMN-PT,[19] and $Na_{1/2}Bi_{1/2}TiO_3$-$BaTiO_3$

a)Author to whom correspondence should be addressed. Electronic mail: veber@icmcb-bordeaux.cnrs.fr

(NBT-BT),[20] respectively. These microstructural features are generally not easily depicted in the case of ceramics.

Achieving centimeter-sized single crystals with controlled composition is our first result. We next show that a cross-over from ferroelectric at large Ti content to relaxor on increasing the Zr/Ti ratio takes place. This is rather a rare case in lead-free ferroelectrics. Although we could achieve piezoelectric coefficients $d_{31} \approx 90$ pC.N^{-1}, we provide evidence that the shift from relaxor state to ferroelectric, one is the key for improved functionality as it is in lead-based materials. We will also provide useful samples for a better understanding of the BCTZ structure, which is still debated in the recent literature.[21–24]

II. CRYSTAL GROWTH AND EXPERIMENTAL PROCEDURE

Raw powders of $BaCO_3$, $CaCO_3$, TiO_2, and ZrO_2 with a purity of more than 99.99% were weighed according to stoichiometrical ratio of the selected BCTZ compositions. After being ground, the mixture of oxide and carbonate coumpounds was heated into a platinum crucible up to 1350 °C for 15 h under air atmosphere in order to synthesize the BCTZ perovskite-structured solid solutions; such reaction parameters were selected from our previous investigations of ceramics.[16]

Three crystal growth attempts were undertaken. The first one was devoted to the $(Ba_{0.850}Ca_{0.150})(Ti_{0.900}Zr_{0.100})O_3$ composition (BCTZ50) owing to its colossal piezoelectric response found in ceramic sample. The last two attempts were achieved with an initial lower zirconium content corresponding to $(Ba_{0.770}Ca_{0.230})(Ti_{0.980}Zr_{0.020})O_3$ and $(Ba_{0.765}Ca_{0.235})(Ti_{0.975}Zr_{0.025})O_3$ formula, respectively. Having brought out the effective segregation of elements during the first growth attempt, the compositions of the second and third liquid solutions were chosen to keep the as-grown crystal composition as close as possible to the targeted perovskite BCTZ50 one. Interestingly, it should be noted that the TiO_2 excess in these two cases compared to BCTZ50 standard composition could play a key role as a self-flux.

At present time, there are only few reports on the crystal growth of $BaTiO_3$-$CaTiO_3$ and $BaTiO_3$-$BaZrO_3$ solid solutions.[25,26] However, there is still no data in the literature dealing with the crystal growth process and the stabilization of the perovskite structure in $BaTiO_3$-$CaTiO_3$-$BaZrO_3$ pseudo-ternary system except for BCTZ relaxor crystal growth carried out recently by Zeng *et al.*[27] Based on these previous works, BCTZ single crystals were grown by using the Top-Seeded Solution Growth method (TSSG). Growth attempts were carried out with an induction furnace. As no suitable seed with BCTZ composition was available, a 3-mm-thick iridium rod was used as a cold thermal point in order to initiate the nucleation and the growth of crystals. The rod was dipped into the melt after homogenization of the liquid solution for 3 h. A rotation speed ranging from 6 to 10 rpm was used with no pulling. The growing crystal mass was monitored during the whole process. The growth attempts took place on decreasing the temperature at a rate ranging between 0.5 °C h^{-1} and 1.5 °C h^{-1}. At the end of the growth process, the boules were set 5 mm above the liquid surface in order to reduce the thermal stress and cooled down to room temperature within 24 h.

Room temperature X-rays powder diffraction experiments were performed on crushed crystals using a PANalytical X'pert MPD diffractometer with θ-θ Bragg Brentano configuration with a backscattering graphite monochromator for CuK_α radiation (λ $CuK\alpha_1 = 1.54056$ Å). The crystal symmetry of the as-grown crystals was then checked and lattice parameters were calculated using a global profile-matching method with the FullProf software. The quality of each profile matching is presented through reliability factors R_p, R_{wp}, R_{exp}, and Chi^2. Laue back-scattering method was used to orientate single crystals. The diffraction patterns were collected using a CCD-camera device (Photonic Science dual lens coupled X-rays Laue system) after a 3–5 min stationary crystal irradiation with polychromatic X-rays supplied by a molybdenum anticathode. Experimental patterns were indexed with OrientExpress software allowing us to orientate crystals within 0.01° of accuracy. Single crystals were then cut with a diamond wire saw. The absolute accuracy of as-cut crystals along a preferential crystallographic direction was finally less than 1°.

Electron Probe Micro-Analysis (EPMA) were achieved with a CAMECA SX-100 apparatus with a wavelength dispersive spectrometer working at 15 kV in order to measure the concentrations of Ba, Ca, Zr, and Ti elements in the perovskite-structured single crystals. Absolute concentration accuracy of elements content was about 0.5 mol. %.

For electrical measurements, the as-grown crystals were cut into crystal wafers along random or [001] crystallographic directions. After the coating of gold electrodes on the major faces using cathodic sputtering technique, a selected BCTZ sample was set in a homemade cell enabling the temperature to be scanned from 100 K up to 450 K. Prior to such low temperature run, the cell was pumped down and a slight overpressure of dry helium was introduced so as to avoid moisture adsorption. The sample was then electrically connected to the output port of an HP4194A impedance analyzer with an operating frequency range of 100 Hz–10 MHz in order to record the complex dielectric permittivity as function of temperature and frequency.

For piezoelectric and pyroelectric measurements, the sample obtained from the third crystal growth attempt (cited as BCTZ3 hereafter) was poled under a DC electric field of about 8–10 kV.cm^{-1} during cooling from the Curie temperature. The piezoelectric constant d_{31} along with corresponding electromechanical coupling coefficient k_{31} for the length thickness extensional mode were determined at different temperatures by the resonance–antiresonance method on the basis of IEEE standards.[28] A digital multimeter Keithley 2100 was used to examine the temperature dependence of both the pyroelectric current and the spontaneous polarization P_s.

III. RESULTS AND DISCUSSION

The crystal growth attempts exhibited saturation temperatures about 1500–1550 °C and yielded centimetre-sized

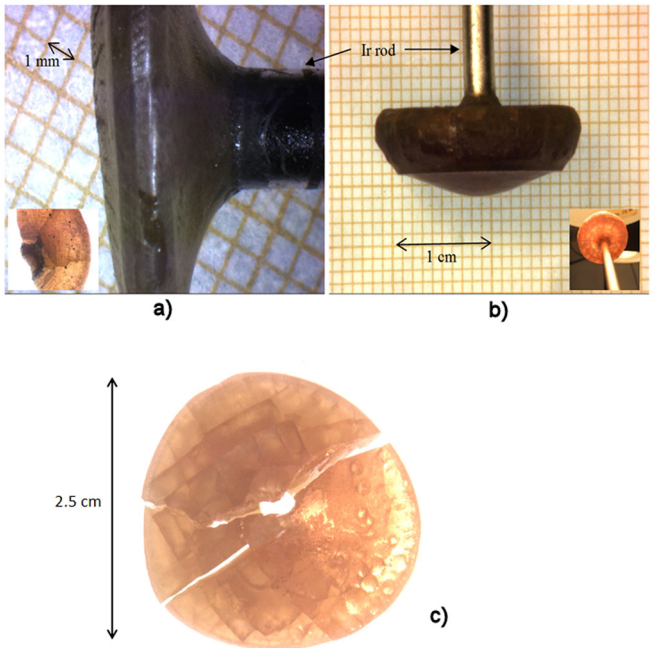

FIG. 1. Centimeter-sized boules obtained after the first (a), second (b), and third (c) crystal growth attempts using the top-seeded solution growth technique. The boules are bordered by radial cracks and show several single crystals around the iridium rod as depicted in insets.

boules delimited by radial cracks (Fig. 1). These boules displayed several single crystals dispersed all around the iridium rod with a cylindrical symmetry. Such obtained morphological features are assumed to be caused by the formation of spontaneous nucleation sites during the growth process around the iridium rod. Transparent and brownish single crystals free of cracks were successfully extracted from the boules. Laue back-scattering patterns for BCTZ1, BCTZ2, and BCTZ3 samples are depicted in Figure 2.

Figure 3(a) shows the X-rays powder diffraction pattern of the as-grown BCTZ1 crystal (first crystal growth attempt) recorded at room temperature. The diffractogram indicates that BCTZ1 is of centrosymmetric cubic perovskite structure. Compared to the targeted BCTZ50 composition, all (hkl) diffraction peaks for BCTZ1 powder are shifted to lower 2θ angles, which correspond to an expansion of the unit cell. The lattice parameters were calculated through the FullProf software and found to be $a = b = c = 4.123(1)$ Å ($R_p = 7.47\%$, $R_{wp} = 9.96\%$, $R_{exp} = 6.47\%$, $Chi^2 = 2.37$). As the single crystal exhibits a slight variation of brownish color (Fig. 1), the minor peak associated to (200) Bragg reflection in Figure 3(b) is assumed to be the contribution of a few amount of flux inclusions within the single crystal. As for BCTZ2 and BCTZ3, which refer to single crystals grown during the second and third attempts, respectively, X-rays powder diffraction analysis shows that the different chemical elements were successfully incorporated into A and B sites of the perovskite to form homogeneous solid solutions. Compared to BCTZ1, a decrease of the unit cell volume has been noticed for the latter compositions. It is revealed by the shift of (h00) Bragg peaks to higher angles (Fig. 3(b)). We can ascribe such a behaviour to the decrease of concentrations of the elements with large ionic radius like Zr and Ba for the given solid solutions.

From the crystallographic point of view, the room temperature XRD patterns of BCTZ2 and BCTZ3 are indexed in the tetragonal symmetry with P4mm space group. Lattice parameters were deduced for BCTZ2 as $a = b = 3.992(9)$ Å, $c = 4.015(8)$ Å ($R_p = 7.67\%$, $R_{wp} = 10.9\%$, $R_{exp} = 8.51\%$, $Chi^2 = 1.64$), and for BCTZ3 $a = b = 4.010(3)$ Å, $c = 4.021(4)$ Å ($R_p = 9.05\%$, $R_{wp} = 12.4\%$, $R_{exp} = 9.26\%$, $Chi^2 = 1.80$). However, it is worth mentioning that the anisotropic line-shape broadenings along with no well-defined peak splitting are the source of considerable difficulty for whole-pattern fitting analysis. As a result, it is complicated to compute accurately lattice parameters of these two compositions. Then, we should not exclude a possible coexistence of different crystallographic structures (multi-dimensional distribution of lattice

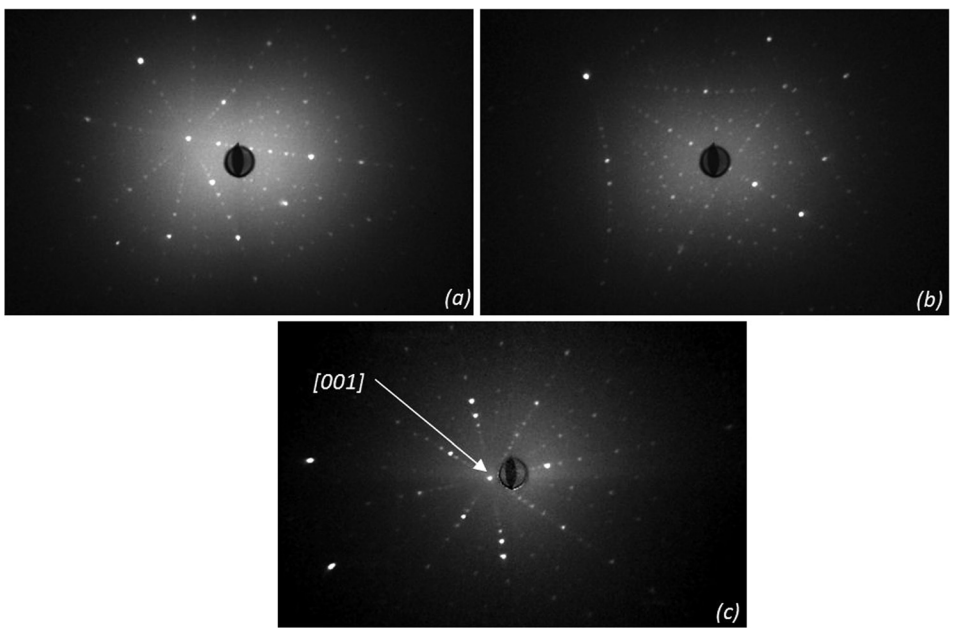

FIG. 2. Laue back-scattering patterns of randomly orientated BCTZ1 (a) and BCTZ2 (b) single crystals. (c) Laue patterns on [001]-orientated BCTZ3 single crystal, which exhibits a 4-fold axis (the sample has been willingly tilted about 5° in order to see the [001] node, as mentioned on the photo).

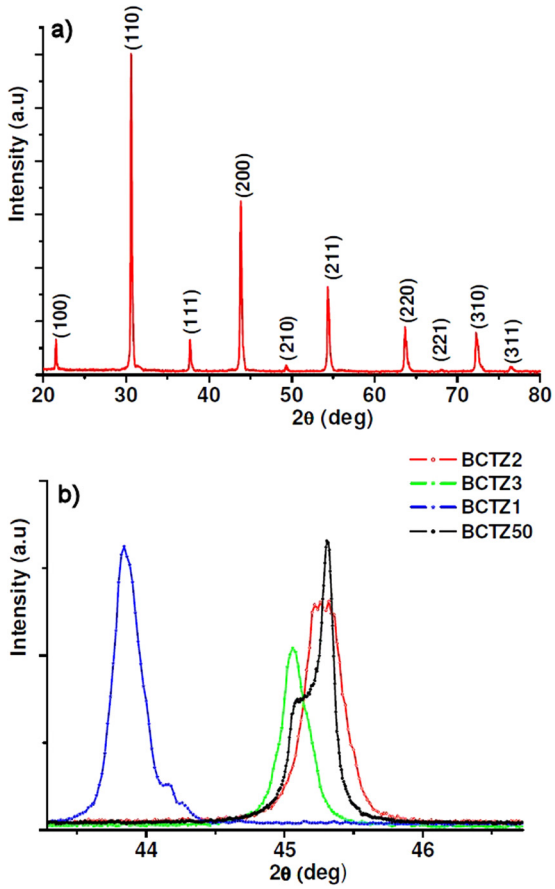

FIG. 3. (a) X-rays powder diffraction pattern of the crushed as-grown BCTZ1 single crystal recorded at room temperature. (b) Shift of the position of the $(200)_{pc}$ diffraction peak showing an increase of the unit cell volume in BCTZ1 compared to BCTZ50 composition. The lattice parameters were calculated using a global profile-matching method and found to be: $a = b = c = 4.123(1)$ Å ($Pm\bar{3}m$ space group) for BCTZ1 and $a = b = 4.000(5)$ Å, $c = 4.017(3)$ Å (P4mm space group) for BCTZ50 ($R_p = 6.88\%$, $R_{wp} = 9.15\%$, $R_{exp} = 6.29\%$, $Chi^2 = 2.11$). Although BCTZ2 and BCTZ3 could be indexed in the tetragonal symmetry (P4mm space group, $a = b = 3.992(9)$ Å, $c = 4.015(8)$ Å for BCTZ2 and $a = b = 4.010(3)$ Å, $c = 4.021(4)$ Å for BCTZ3), a possible coexistence of different symmetries should not be excluded in these two compositions because of anisotropic line-shape broadenings along with no well defined peak splitting.

metrics). High resolution XRD experiments are obviously required to provide unambiguous response to a such puzzling situation.

Being consistent with XRD characterizations, chemical analysis performed on BCTZ1 and BCTZ2 single crystals give, respectively $(Ba_{0.953}Ca_{0.047})(Ti_{0.427}Zr_{0.573})O_3$ (sample 1) and $(Ba_{0.857}Ca_{0.143})(Ti_{0.928}Zr_{0.072})O_3$ (sample 2) average compositions. This shows that the actual compositions are far away from the targeted one $(Ba_{0.850}Ca_{0.150})(Ti_{0.900}Zr_{0.100})O_3$ (BCTZ50). We ascribe such deviations to the poor knowledge of the phase diagram as well as to selective segregation of the elements. In order to drive the final crystal growth experiment composition starting from a given load composition, we actually anticipated the segregation that will unsurprisingly take place during the growth: the effective segregation of elements depends on the initial composition of the liquid bath. Indeed, Zr^{4+} and Ba^{2+} cations were incorporated into the crystals in higher contents than their initial ones in the liquid solution. However, Ca^{2+} and Ti^{4+} contents generally exhibited an opposite trend. Molar concentrations of elements for the third attempt were systematically calculated from the linear regression fitted curves deduced from the chemical analysis of BCTZ1 and BCTZ2 single crystals with respect to their initial liquid compositions. We plotted in Figure 4 as dashed lines, the targeted Ba, Ti, Zr, and Ca contents, which underline that BCTZ3 was indeed close to the optimal range $(Ba_{0.838}Ca_{0.162})(Ti_{0.854}Zr_{0.146})O_3$ by comparison with $(Ba_{0.850}Ca_{0.150})(Ti_{0.900}Zr_{0.100})O_3$. In this case, we were also capable to get well oriented parallel plate samples owing to an enhanced homogeneity of bigger boule.

BCTZ1 sample was cut from the as-grown crystals and polished to optical quality for dielectric measurements. The sample is a plate of dimensions $4.7 \times 1.5 \times 0.61$ mm^3. The temperature dependence of the real ε'_r and imaginary ε''_r components of the complex dielectric permittivity are displayed in Figure 5, showing the whole frequencies range between 1 kHz and 7 MHz. Both these parameters illustrate the usual trends of relaxor. ε'_r and ε''_r are frequency independent at high temperature and ε'_r increases on cooling. Such increase follows the Curie-Weiss law with a deviation from this law at $T_d \approx 190$ K. Moreover, ε'_r undergoes a broad peak whose corresponding temperature T_m increases, while the amplitude ε'_{rmax} decreases with increasing frequency. At temperatures lower than this maximum, ε'_r curves are dispersed and parallel. The imaginary part of the relative dielectric constant displays frequency dependent maxima whose amplitude increases with the operating frequency, i.e., opposite to the real part. All these qualitative features are in perfect agreement with the archetype relaxor compound PMN.[29,34] A more quantitative insight can be obtained from the plot of the frequency versus the dielectric maximum temperature in Arrhenius scale (Fig. 6(a)). The linear variation in the plot shows that the relaxation process is thermally activated $f = f_0 \exp(-E_a/kT)$ with an activation energy $Ea = 0.26$ eV and a frequency prefactor $f_0 = 1.4 \times 10^{14}$ Hz. Due to the limited frequency points, we were not capable to

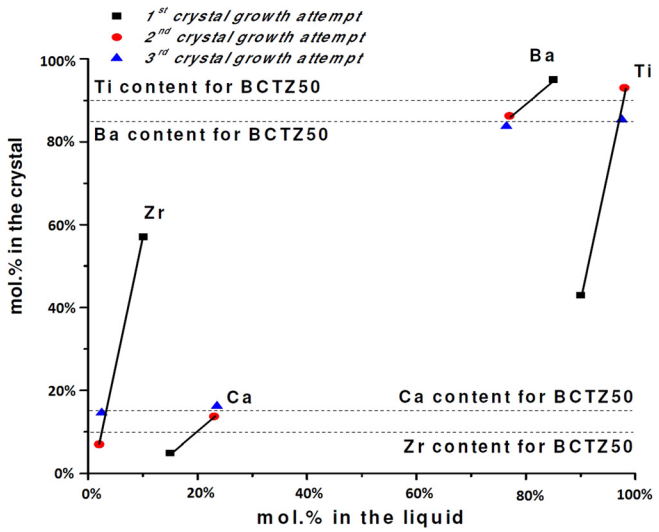

FIG. 4. Molar concentrations of elements per site for BCTZ single crystals as a function of those corresponding to their initial liquid compositions. Dashed lines represent the Ca, Ba, Ti, and Zr contents corresponding to BCTZ50 composition.

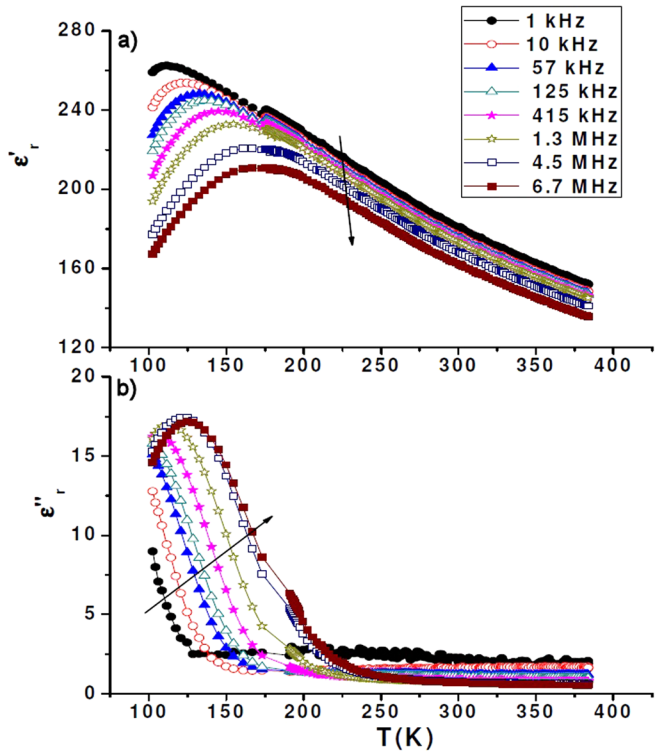

FIG. 5. Real and imaginary parts of the complex dielectric permittivity, ε'_r and ε''_r, respectively, as a function of temperature and frequency for BCTZ1 with (100) main faces parallel to the growth direction (arrows indicate the direction of increasing frequency).

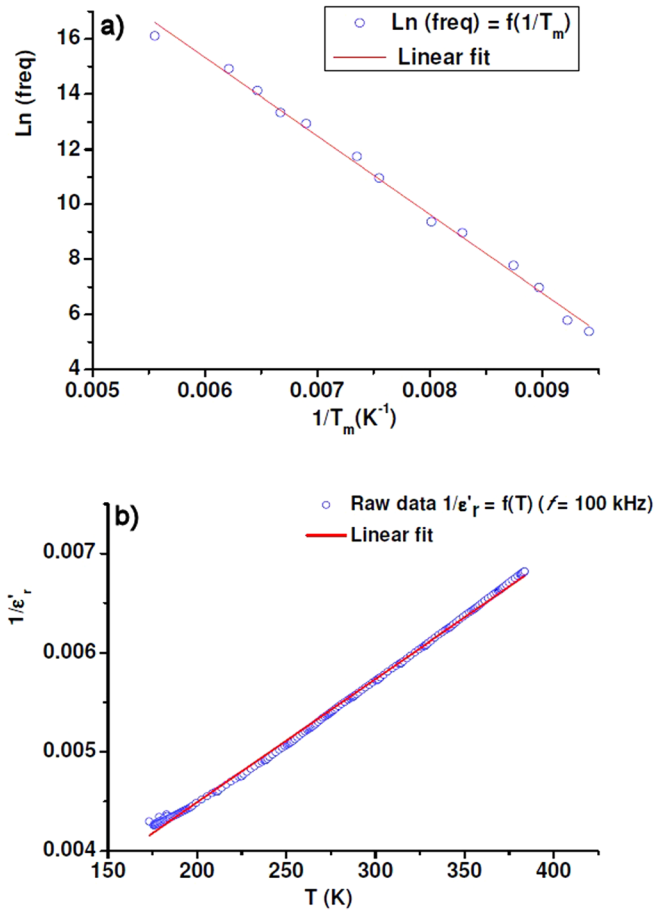

FIG. 6. (a) Arrhenius plot of the operating frequency as a function of the temperature at which the dielectric maxima occur. The red line is the fitted line of the Arrhenius law. (b) Reciprocal dielectric permittivity $1/\varepsilon'_r$ for BCTZ1 shows a deviation from linear response at low temperatures. The temperature (T_d) corresponding to such deviation is much higher than the dynamic transition temperature T_m. The red line shows a fit to the Curie Weiss law.

observe the frequency bending in Arrhenius scale that would provide Vogel Fulcher temperature. T_{VF} can be viewed as the static dipolar freezing temperature for the relaxation process.[29]

In addition, a quantitative agreement with relaxor trends can be found in the already mentioned Curie Weiss fit of the real part of the dielectric permittivity $\varepsilon'_r = C/(T\text{-}T_c)$, where the fitting parameters are the Curie constant $C = 7.9 \times 10^4$ K and the Curie temperature $T_c = 147$ K (at $f = 125$ kHz). The Curie constant is below 10^5 K as observed in many relaxors, while it is more than 10^5 K in ferroelectrics. In the present case, the Curie temperature is 147 K, while the dielectric maximum appears at 132 K (Fig. 6(b)); such disagreement between these two characteristic temperatures is also a confirmation of the relaxor feature in the BCTZ1 single crystal.

Referring to the systematic investigation of the $BaTiO_3$-$CaTiO_3$-$BaZrO_3$ phase diagram of powders and ceramics,[30] we find a good agreement between the Zr and Ba segregation in BCTZ single crystals and their relaxor features. Indeed, when the Zr content at B-sites of the perovskite exceeds 27 mol. %, a shift from ferroelectric to relaxor state is observed. So, starting from the initial ferroelectric composition with Zr content = 15 mol. %, we obtained a relaxor one with Zr content = 57 mol. %. It is worth mentioning that finding lead-free relaxor single crystal is itself an interesting achievement, since the number of such functional materials (free of lead) is quite restricted.

Random fields and random strains have been believed for a long time to be the main mechanisms responsible for the relaxor behavior in disordered perovskite solid solutions.[31–33] Spatial fluctuations of these interactions result in the formation of polar nanoregions (PNRs), which appear because of chemical short-range ordering effects.[34] Recently, Akbarzadeh *et al.* have rejected this model on the basis of first-principles investigations of Ba(Ti, Zr)O_3 disordered perovskite. They have demonstrated that the difference in ferroelectric strength between Ti^{4+} and Zr^{4+} cations along with chemical heterogeneities (some regions of space can be more Ti rich than others) are the main source of the relaxor behavior in $Ba(Zr_{0.5}Ti_{0.5})O_3$.[35] In this work, we think that the substitution of barium (Ba^{2+}) by calcium (Ca^{2+}) stabilizes more and more the perovskite structure but it does not alter significantly functional properties of BCTZ solid solutions: relaxor-characteristic signatures are solely governed by the Zr content in B-sites.

We discuss now the dielectric behavior of the randomly oriented BCTZ2 sample of composition $(Ba_{0.857}Ca_{0.143})(Ti_{0.928}Zr_{0.072})O_3$, which contains a much higher Ti content than the already presented BCTZ1 relaxor crystal. As plotted in Figure 7, both dielectric constant ε'_r and loss $\tan\delta$ display broad frequency-independent anomalies at 310 K and 275 K. These two peaks are the signature of two successive phase transitions, which are in full agreement with what was

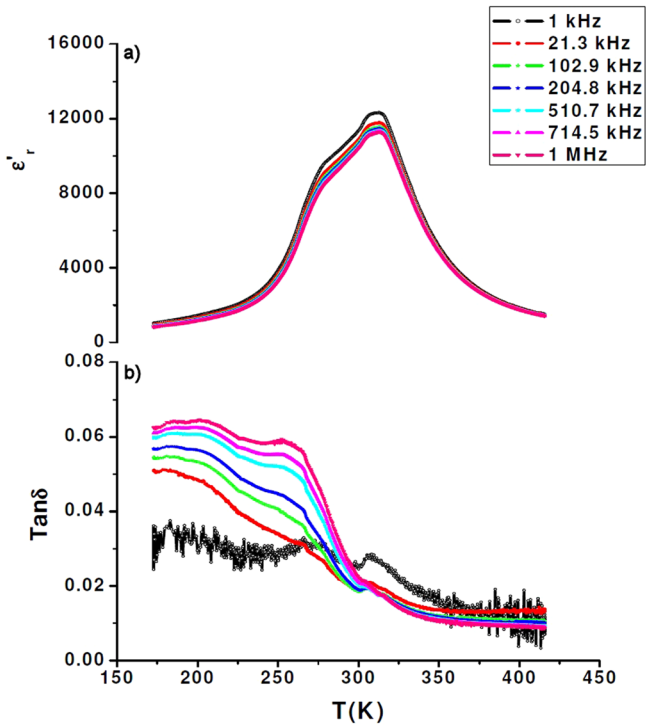

FIG. 7. Dielectric constant ε'_r and loss tangent ($\tan\delta$) as a function of temperature and frequency for a randomly oriented BCTZ2 sample.

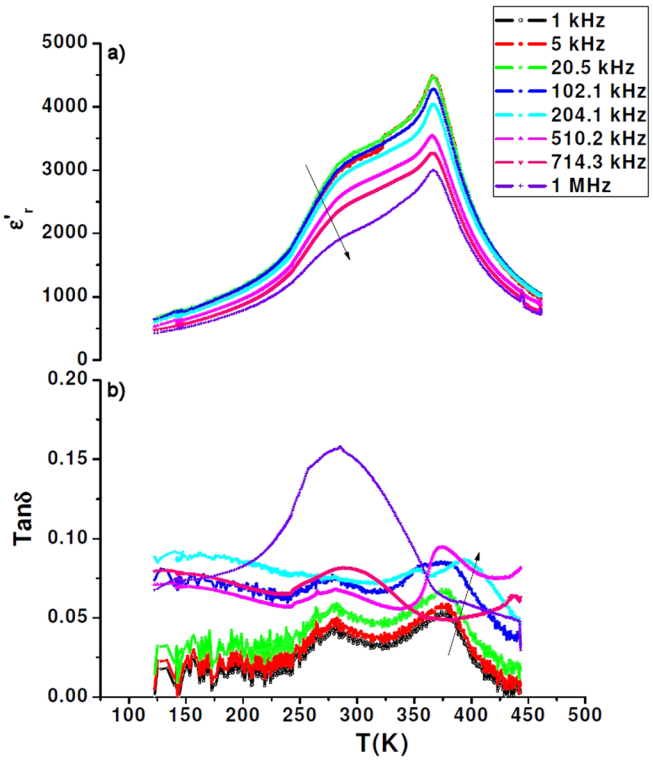

FIG. 8. Temperature dependence of dielectric constant ε'_r and loss tangent ($\tan\delta$) at various frequencies for [001] oriented BCTZ3 single crystal (arrows indicate the direction of increasing frequency).

reported in ceramics of similar composition. We thus conclude that even though non-congruent melting is a limiting factor for an accurate control of crystal compositions, we succeeded to achieve a relaxor to ferroelectric continuous cross-over, which is consistent with the well-established phase diagram of BCTZ ceramics.[30] Thanks to this property tuning, we are now capable to focus our investigations on composition in the proximity to that with the highest piezoelectric coefficient $(Ba_{0.850}Ca_{0.150})(Ti_{0.900}Zr_{0.100})O_3$.

Figure 8 shows the temperature dependence of the dielectric constant ε'_r and loss $\tan\delta$ at various frequencies for [001]-oriented BCTZ3 single crystal. Dielectric parameters confirmed the chemical analysis displaying well defined anomalies at 366 K and 265 K. The intermediate phase was thus much more extended than that depicted in BCTZ2, which was already ferroelectric. In agreement with ceramics phase diagram, this extended stability range of the tetragonal state proves that we are approaching the interesting composition.[21] Another feature, which was not observed in ceramics, is the very peculiar frequency behavior of the dielectric permittivity. While it is almost dispersion-less in the high temperature cubic phase and in the low temperature phases, it shows a strong dispersion in the vicinity of dielectric anomalies. Even though the temperature at which the anomalies occur is not frequency dependent, a strong depletion of the permittivity is observed when the frequency increases. Such phenomena could be attributed to ferroelectric domain wall motions, which translate into an increasing of the dielectric loss with increasing frequency.

In BCTZ solid solutions, we naturally expect compositional fluctuations and/or structural disordering of cations in one or more crystallographic sites of the perovskite structure. These microscopic characteristics will systematically disturb the long-range dipolar interactions and induce a diffuse behavior within the ferroelectric phase. The strong dispersion observed in both dielectric parameters (Fig. 8) could be then understood as a signature of the coexistence of two polar states. In agreement with recent established models, such coexistence will favor multiple polarization pathways in a strongly degenerate free energy landscape: in fact, structural disordering/instabilities induced by local chemical inhomogeneities cause polarization direction of the ferroelectric domains to be decoupled from crystal lattice (drastic lowering of the polarization anisotropy energy). The polar domains may have irregular shapes leading to high polarization flexibility under external stresses and, consequently, to a large piezoelectric response.[14,15,36]

Pyroelectric and piezoelectric measurements were performed on [001] oriented BCTZ3 single crystal. The sample was a plate of 1.41 × 1 mm^2 and 0.58 mm-thick. Figure 9 illustrates the temperature dependence of the pyroelectric coefficient p along with the spontaneous polarization P_s. Two anomalies are detected corresponding to cubic-tetragonal-rhombohedral phase transitions. Contrary to what has already been observed in BCTZ ceramic samples,[16] Ps shows less sensitivity to the temperature change in BCTZ3 single crystal. The maximum polarization remains however below 20 $\mu C\ cm^{-2}$.

The piezoelectric response for the length thickness extensional mode is determined at different temperatures through frequency-dependent sweeps of the conductance G and the susceptance B (Fig. 10). Table I summarizes results obtained for three selected temperatures.

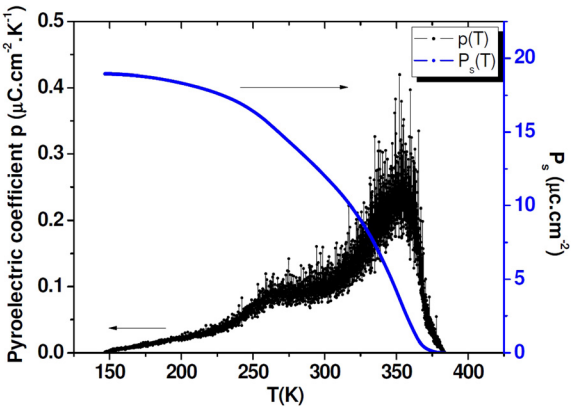

FIG. 9. Temperature dependence of the pyroelectric coefficient p and spontaneous polarization P_s of the [001] oriented BCTZ3 single crystal.

It can be seen that the electromechanical response of BCTZ3 is smaller than that observed in BCTZ50 ceramic sample close to room temperature ($d_{31\ (BCTZ50\ ceramic\ disk)} > d_{31\ (BCTZ3\ single\ crystal\ plate)}$ near RT). Some possibilities can be suggested to understand such a difference:

(1) Common resonance geometries along with recommended aspect ratios are usually used to characterize piezoelectric materials. The aspect ratio is chosen to ensure that the modes of resonance are well separated and that the desired motion is primarily in the specified direction. In our case, the dimensions of BCTZ3 single crystal do not follow appropriately the metric conditions for length thickness extensional mode. Therefore, we may introduce a significant error when determining the electromechanical coefficients.
(2) The ferroelectric and piezoelectric responses possess anisotropic behaviors in single crystals and optimized crystallographic orientation is required to increase the piezoelectric efficiency.[7,37,38]
(3) Although the BCTZ3 composition is close to the targeted BCTZ50 from the chemical point of view, both of them behave differently from the crystallographic point of view. Based on recent studies of Keeble *et al.*; the orthorhombic O-phase found in BCTZ50 close to ambient temperature seems to be absent in BCTZ3 (from dielectric and pyroelectric measurements). Consequently, BCTZ3 is far away from the phase convergence region already reported for BTZ-BCT pseudo-binary phase diagram and no instability gradient could then be attained. This situation may explain the relatively low piezoelectric response in BCTZ3 compared to BCTZ50 ceramics composition.[21]

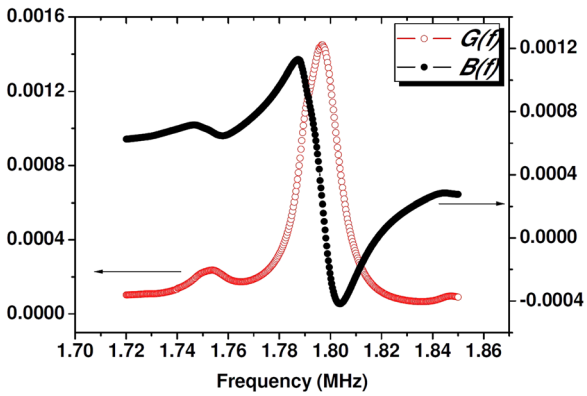

FIG. 10. Resonance curves for the length thickness extensional mode measured at 337 K for [001] oriented BCTZ3 single crystal. The plot shows a frequency-dependent sweep of the conductance G and the susceptance B, which are the real and imaginary components of the admittance, respectively.

TABLE I. Piezoelectric constants d_{31} and electromechanical coupling factors k_{31} calculated at three selected temperatures for BCTZ3 crystal wafer oriented along pseudo-cubic [001] direction.

T (K)	d_{31} (pC.N^{-1})	k_{31}
293	70	0.14
305	93	0.18
337	91	0.17

Finally, it is perhaps interesting to state that electromechanical properties of BCTZ3 single crystal presented, in this work, are consistent with those reported for BTZ ($BaTiO_3$-$BaZrO_3$) and BCT ($BaTiO_3$-$CaTiO_3$) single crystals synthesized by Laser Heated Pedestal Growth and Floating Zone techniques, respectively.[25,26]

IV. CONCLUSIONS

BCTZ single crystals have been successfully grown in the $BaTiO_3$-$CaTiO_3$-$BaZrO_3$ pseudo-ternary system. The X-rays powder diffraction and EPMA analysis revealed that the as-grown crystals are enriched with zirconium and barium due to the difference of segregation of cations in the solution. Our first two attempts showed that a continuous cross-over from relaxor to ferroelectric state can be achieved in BCTZ lead-free materials. This result could be considered as a first step toward further optimization of the piezoelectric properties of BCTZ single crystals. Indeed, in lead-containing materials like PMN, it was the relaxor properties of PMN, which were the basis ground of the unprecedented piezoelectric activity in the PMN-PT solid solutions as the $PbTiO_3$ content was raised. In addition, the relaxor state may be considered as a mixing of many local polarizations (PNRs) within an overall cubic symmetry. The reduction of Zr content may refine the size of polar nanoregions and enhance their self-organization similarly to what recently observed in NBT-BT single crystals.[20] Such compositionally driven evolution of the domain structures can lead to extremely large piezoelectric coefficients in BCTZ system.

Based on three growth trials, we were able to tune the starting composition to reach $(Ba_{0.838}Ca_{0.162})(Ti_{0.854}Zr_{0.146})O_3$, which is very close to the best piezoelectric composition BCTZ50. This single crystal (BCTZ3) seems to display very interesting coexistence between ferroelectric and relaxor states, which lead to a reasonably high transverse piezoelectric coefficient $d_{31} = 93$ pC.N^{-1} near room temperature. Further growth attempts using these BCTZ single crystals as a seed will enable us to increase the size and the homogeneity of the boules, thus allowing an improvement of samples

shape for piezoelectric measurements. We suggest that this interesting coexistence of two polar states in BCTZ perovskite solid solutions will foster the interest for in-depth investigations of their crystal/domain structures from the average to local levels. This is of interest not only for lead-free but also for classical lead-containing piezoelectrics.

ACKNOWLEDGMENTS

In the framework of the research and development of functional materials, the authors acknowledge GIS–Advanced Material in Aquitaine (AMA) for its logistical support.

[1]K. M. Rabe, C. H. Ahn, and J.-M. Triscone, *Physics of Ferroelectrics: A Modern Perspective* (Springer, Berlin, 2007).
[2]J. Kreisel, B. Noheda, and B. Dkhil, Phase Trans. **82**, 633 (2009).
[3]R. H. Mitchell, *Perovskites: Modern and Ancient* (Almaz Press, Ontario, 2002).
[4]B. Noheda, D. E. Cox, G. Shirane, J. A. Gonzalo, L. E. Cross, and S. E. Park, Appl. Phys. Lett. **74**, 2059 (1999).
[5]B. Noheda, Curr. Opin. Solid State Mater. Sci. **6**, 27 (2002).
[6]Z.-G. Ye, Y. Bing, J. Gao, A. A. Bokov, P. Stephens, B. Noheda, and G. Shirane, Phys. Rev. B **67**, 104104 (2003).
[7]S.-E. Park and T. R. Shrout, J. Appl. Phys. **82**, 1804 (1997).
[8]S.-E. Park and W. Hackenberger, Curr. Opin. Solid State Mater. Sci. **6**, 11 (2002).
[9]Q. Zhang, Y. Zhang, F. Wang, Y. Wang, D. Lin, X. Zhao, H. Luo, W. Ge, and D. Viehland, Appl. Phys. Lett. **95**, 102904 (2009).
[10]W. Ge, H. Liu, X. Zhao, B. Fang, X. Li, F. Wang, D. Zhou, P. Yu, X. Pan, D. Lin, and H. Luo, J. Phys. D: Appl. Phys. **41**, 115403 (2008).
[11]H.-Y. Park, C.-W. Ahn, H.-C. Song, J.-H. Lee, S. Nahm, K. Uchino, H.-G. Lee, and H.-J. Lee, Appl. Phys. Lett. **89**, 062906 (2006).
[12]Y. Saito, H. Takao, T. Tani, T. Nonoyama, K. Takatori, T. Homma, T. Nagaya, and M. Nakamura, Nature (London) **432**, 84 (2004).
[13]M. Prakasam, P. Veber, O. Viraphong, L. Etienne, M. Lahaye, S. Pechev, E. Lebraud, K. Shimamura, and M. Maglione, Comptes Rendus Phys. **14**(2–3), 133–140 (2013).
[14]D. Damjanovic, Appl. Phys. Lett. **97**, 062906 (2010).
[15]W. Liu and X. Ren, Phys. Rev. Lett. **103**, 257602 (2009).
[16]F. Benabdallah, A. Simon, H. Khemakhem, C. Elissalde, and M. Maglione, J. Appl. Phys. **109**, 124116 (2011).
[17]D. Phelan, X. Long, Y. Xie, Z.-G. Ye, A. M. Glazer, H. Yokota, P. A. Thomas, and P. M. Gehring, Phys. Rev. Lett. **105**, 207601 (2010).
[18]A. A. Bokov, X. Long, and Z.-G. Ye, Phys. Rev. B **81**, 172103 (2010).
[19]F. Fang, X. Luo, and W. Yang, Phys. Rev. B **79**, 174118 (2009).
[20]J. Yao, L. Yan, W. Ge, L. Luo, J. Li, D. Viehland, Q. Zhang, and H. Luo, Phys. Rev. B **83**, 054107 (2011).
[21]D. S. Keeble, F. Benabdallah, P. A. Thomas, M. Maglione, and J. Kreisel, Appl. Phys. Lett. **102**, 092903 (2013).
[22]A. B. Haugen, J. S. Forrester, D. Damjanovic, B. Li, K. J. Bowman, and J. L. Jones, J. Appl. Phys. **113**, 014103 (2013).
[23]J. Gao, D. Xue, Y. Wang, D. Wang, L. Zhang, H. Wu, S. Guo, H. Bao, C. Zhou, W. Liu, S. Hou, G. Xiao, and X. Ren, Appl. Phys. Lett. **99**, 092901 (2011).
[24]D. Damjanovic, A. Biancoli, L. Batooli, A. Vahabzadeh, and J. Trodahl, Appl. Phys. Lett. **100**, 192907 (2012).
[25]D. Fu, M. Itoh, and S.-y. Koshihara, Appl. Phys. Lett. **93**, 012904 (2008).
[26]Z. Yu, R. Guo, and A. S. Bhalla, Appl. Phys. Lett. **77**(10), 1535 (2000).
[27]Y. Zeng, Y. Zheng, X. Tu, Z. Lu, and E. Shi, J. Cryst. Growth **343**, 17–20 (2012).
[28]ANSI/IEEE Std. 176-1987, "IEEE Standard on Piezoelectricity".
[29]R. Waser, U. Böttger, and S. Tiedke, *Polar Oxides Properties, Characterization, and Imaging* (Wiley-VCH Verlag GmbH & Co. KGaA, Weinheim, 2005).
[30]J. Ravez, C. Broustera, and A. Simon, J. Mater. Chem. **9**, 1609–1613 (1999).
[31]V. Westphal, W. Kleemann, and M. D. Glinchuk, Phys. Rev. Lett. **68**, 847 (1992).
[32]R. Blinc, A. Gregorovič, B. Zalar, R. Pirc, V. V. Laguta, and M. D. Glinchuk, Phys. Rev. B **63**, 024104 (2000).
[33]B. E. Vugmeister and M. D. Glinchuk, Rev. Mod. Phys. **62**, 993 (1990).
[34]A. A. Bokov and Z.-G. Ye, J. Mater. Sci. **41**, 31–52 (2006).
[35]A. R. Akbarzadeh, S. Prosandeev, E. J. Walter, A. Al-Barakaty, and L. Bellaiche, Phys. Rev. Lett. **108**, 257601 (2012).
[36]G. A. Rossetti, Jr., A. G. Khachaturyan, G. Akcay, and Y. Ni, J. Appl. Phys. **103**, 114113 (2008).
[37]S. Wada, K. Takeda, T. Muraishi, H. Kakemoto, T. Tsurumi, and T. Kimura, Ferroelectrics **373**, 11 (2008).
[38]S.-E. Park, S. Wada, L. E. Cross, and T. R. Shrout, J. Appl. Phys. **86**, 2746 (1999).